The pore structure of *Clostridium perfringens* epsilon toxin

Christos G. Savva[1], Alice R. Clark[2], Claire E. Naylor[3], Michel R. Popoff[4], David S. Moss[5], Ajit K. Basak[5], Richard W. Titball[6] and Monika Bokori-Brown[6]

[1]Leicester Institute of Structural and Chemical Biology, Department of Molecular and Cell Biology, University of Leicester, Lancaster Road, Leicester LE1 7HB, UK

[2]Faculty of Science and Engineering, University of Wolverhampton, Wulfruna Street, Wolverhampton WV1 1LY, UK

[3]Molecular Dimensions, Willie Snaith Road, Newmarket, CB8 7SQ, UK

[4]Bactéries Anaérobies et Toxines, Institut Pasteur, 25-28 Rue du Docteur Roux, 75724 Paris CEDEX 15, France

[5]Department of Biological Sciences, Birkbeck College, Malet Street, London, WC1E 7HX, UK

[6]College of Life and Environmental Sciences, University of Exeter, Stocker Road, Exeter, EX4 4QD, UK

Correspondence and requests for materials should be addressed to M.B.-B. (email: m.bokori-brown@exeter.ac.uk)

Abstract

Epsilon toxin (Etx), a potent pore forming toxin (PFT) produced by *Clostridium perfringens*, is responsible for the pathogenesis of enterotoxaemia of ruminants and has been suggested to play a role in multiple sclerosis in humans. Etx is a member of the aerolysin family of β-PFTs (aβ-PFTs). While the Etx soluble monomer structure was solved in 2004, Etx pore structure has remained elusive due to the difficulty of isolating the pore complex. Here we show the cryo-electron microscopy structure of Etx pore assembled on the membrane of susceptible cells. The pore structure explains important mutant phenotypes and suggests that the double β-barrel, a common feature of the aβ-PFTs, may be an important structural element in driving efficient pore formation. These insights provide the framework for the development of novel therapeutics to prevent human and animal infections, and are relevant for nano-biotechnology applications.

Introduction

Epsilon toxin (Etx) is a pore forming toxin (PFT) produced by *Clostridium perfringens* type B and D strains and plays an important role in the pathogenesis of enterotoxaemia, a severe neurological disease of domestic ruminants, particularly sheep. More recently, Etx has been implicated in the development of multiple sclerosis (MS) in humans[1, 2, 3].

Etx is typically secreted by the bacterium in the gut as a relatively inactive, water-soluble monomer, called protoxin (P-Etx), with an estimated molecular weight of 32.9 kDa[4]. The protoxin is converted to the active, mature toxin after carboxy- and amino-termini peptides are removed by proteolytic cleavage in the gut, either by digestive proteases of the host, such as trypsin, or protease produced by *C. perfringens*[5]. Toxin activation generates a more acidic protein (isoelectric point of 5.4 vs 8.3) that is nearly 1,000 times more toxic than its progenitor[6, 7]. By a mechanism unknown, Etx crosses the gut wall, enters the blood stream and accumulates preferentially in the brain and kidneys[8, 9].

Etx is a member of the aerolysin family of β-pore-forming toxins (aβ-PFTs). Members of the aβ-PFTs are found in all kingdoms of life and can be used for either attack or defence[10, 11]. Other bacterial toxins from the aβ-PFTs that play a role in disease include aerolysin from the human pathogen *Aeromonas hydrophila*[12], enterotoxin (CPE) from *C. perfringens*[13], α-toxin from *Clostridium septicum*[14], and monalysin from *Pseudomonas entomophila*[15]. Other members of the aβ-PFTs serve in defence, such as lysenin produced by immune cells of the earthworm *Eisenia fetida*[16], assist in prey digestion, such as

hydralysins from *Cnidaria*[17], or have cytocidal activity against human cancer cells, such as parasporin-2 from *Bacillus thuringiensis*[18].

As evidenced by their crystal structures, members of the aβ-PFTs share an overall similar domain arrangement[11]. They typically contain one or more receptor binding domains (RBD) and a pore forming module (PFM), a well conserved structural element of the aβ-PFTs[11, 19]. The PFM, rich in serine and threonine residues, contains a flexible membrane insertion loop flanked by pre-insertion strands that refold into an amphipathic β-hairpin during pore formation to create the transmembrane β-barrel of the pore[20].

The crystal structure of the water-soluble, monomeric P-Etx was solved by Cole *et al.* in 2004[21] and revealed an elongated molecule composed mainly of β-sheets, with two strands traversing the entire molecule. The suggested RBD at the amino-terminus contains a cluster of surface exposed aromatic amino acids critical for cell binding[22, 23], and the PFM at the carboxy-terminus is suggested to play a role in oligomerization and pore formation[11, 19]. The PFM also contains a C-terminal peptide (CTP), proteolytic removal of which is essential for toxin activation[6] as interaction of the CTP with the pre-insertion strands restricts their movement, thus preventing pore formation[20]. A glycan (β-octyl-glucoside) binding site has also recently been identified in the PFM, suggesting that Etx may have two distinct receptor binding sites[22].

Etx is unique amongst aβ-PFTs as it shows high potency and high cell specificity. The 50% lethal dose (LD_{50}) in mice after intravenous administration of the toxin is reported to

be 100 ng kg^{-1} [24], equivalent to 7 µg per 70 kg human. This makes Etx the third most potent clostridial toxin after botulinum and tetanus neurotoxins[24]. For this reason, the toxin is classified as a potential biological weapon in some countries and as a category B biological agent by the U.S. public health body, the Centers for Disease Control and Prevention (CDC)[25]. Among the many cell lines tested, only a few are susceptible to Etx. Most in vitro studies on Etx, including this study, have been carried out using the Madin-Darby Canine Kidney (MDCK) cell line as this cell line is the most sensitive to the toxin[26, 27, 28, 29]. The cell specificity of Etx suggests that the toxin binds to a specific receptor in the membrane of target cells and this is likely to explain why the toxin is over 1,000 times more potent compared to other aβ-PFTs.

To date, two putative Etx receptors have been identified: the O-linked glycoprotein hepatitis A virus cellular receptor 1 (HAVCR1)[23] and the tetraspan membrane proteolipid myelin and lymphocyte protein (MAL)[2]. The molecular basis for the interaction of these putative receptors with Etx remains unknown, although it is thought that the binding site for Etx on the glycoprotein HAVCR1 includes one of the sugar components, while in MAL the second extracellular loop is critical for binding and cytotoxicity of Etx. Etx can also interact with artificial lipid bilayers and form functional pores without the help of receptors, albeit with less efficiency[30, 31, 32].

Both inactive P-Etx and activated toxin can bind to cells but only activated toxin with CTP removed can form heptameric pre-pores on the membrane surface in the next step of pore formation[33]. Finally, the heptamer, with a molecular mass of approximately 155-174

kDa[2, 28, 29, 34], inserts into the membrane, which is triggered by significant structural rearrangements within the PFM of each protomer in the complex. Pore formation disrupts the membrane and is central to the damage caused to intoxicated cells, and consequently to the symptoms of disease due to the leakage of water and small ions through the pores that may lead to cell death.

Whilst atomic resolution structures of the water-soluble, monomeric forms have been determined for many members of the aβ-PFTs over the past few decades, their corresponding pore structures have only recently been revealed. The lysenin pore was the first high-resolution structure of the aβ-PFTs[20, 35]. A 3.9 Å structure of the aerolysin pre-pore and a 7.5 Å structure of aerolysin pore have also been determined[36].

The cryo-electron microscopy (cryo-EM) structure of Etx pore determined here provides further insights into the molecular details of structural rearrangements during the pore formation process of the aβ-PFTs. These results will have important implications for the development of novel therapeutics aimed at the functional disruption of pore formation to prevent human and animal diseases, and are relevant for nano-biotechnology applications.

Results

Isolation of the Etx pore

The formation of biologically active oligomers has been a limiting factor for obtaining structural information of the pore form of Etx. Unlike aerolysin[37, 38], Etx does not spontaneously oligomerize into SDS-resistant species when activated in aqueous buffer, and negatively stained EM samples do not reveal regular particles other than elongated monomers and small clumps (Supplementary Figure 1a). Furthermore, efficient oligomerization cannot be promoted by the addition of liposomes of various lipid compositions or detergent micelles. The uncertainty in receptor identity combined with the high cell specificity of Etx prompted us to investigate if the pores could be assembled on susceptible cells and then purified for structural studies. We assembled Etx oligomers that were biologically active towards Super Dome cells, a clone of MDCK cells that forms domes that are approximately five times the area of MDCK cells, thus exhibiting exceptional sensitivity to Etx[39]. The cytotoxic activity of trypsin activated recombinant wild type Etx towards Super Dome cells was measured using a lactate dehydrogenase (LDH) assay. The average dose of recombinant Etx required to kill 50% of Super Dome cells (CT_{50}) was 2.47 ± 0.47 nM (S.E.M.) or 78.27 ± 14.89 ng ml^{-1} (S.E.M.) (Figure 1a). Etx monomers oligomerised and formed SDS-resistant pores of an apparent molecular weight of ~155 kDa on the membrane of Super Dome cells (Figure 1b), consistent with previous studies[2, 28, 29, 34]. Subsequently, the complexes were solubilised in detergent and treated as single particles for cryo-EM analysis. Solubility screening using ultracentrifugation identified *n*-dodecyl-β-D-maltoside (DDM) as a suitable detergent,

144 which has previously been successfully used to solubilize lysenin and Etx pores[20, 34, 35]
145 (Supplementary Figure 2).
146
147 **Structural determination of the Etx pore**
148 When observed using transmission electron microscopy (TEM), the isolated Etx material
149 appeared heterogeneous. The extremely low yields (~10 μg from 6 x 10^8 cells) meant we
150 could not pursue additional clean-up steps, such as size-exclusion chromatography. This
151 heterogeneity hindered particle identification and selection using manual or automated
152 picking procedures (Supplementary Figures 3, 4). Despite this, an initial dataset of 613
153 micrographs resulted in ~14,000 particles after 2D and 3D classification clean-up steps
154 and produced a map which reached 4.6 Å, at which resolution the β-strands just begin to
155 separate (Supplementary Figure 3, inset). We reasoned that the use of a Volta Phase Plate
156 (VPP) would be advantageous for two reasons. First, the contrast of the protein
157 component would increase, aiding particle picking and alignment. Second, the number of
158 particles required to achieve a high-resolution structure could decrease as compared to
159 conventional defocused data[40]. Therefore, we proceeded to image the exact same grid
160 used before with the VPP. Although the samples still appeared heterogeneous (Figure
161 2a), approximately two times as many particles remained after clean-up steps as
162 compared to the non-VPP dataset from a dataset that was only 25% larger. This resulted
163 in a final map at an overall resolution of 3.2 Å (Figure 2c, d and Supplementary Figure
164 5). Estimation of the B-factors for both datasets indicated that the phase plate data was
165 indeed of higher quality when comparing the same number of particles used in a
166 reconstruction (Supplementary Figure 6).

Architecture of the Etx pore

The atomic model of the Etx pore is shown in Figure 3a, b. The overall architecture of the Etx pore resembles that of its structural homologues lysenin[20, 35] and aerolysin[36], with a β-barrel that spans the height of the molecule, a motif that so far seems specific for the aβ-PFTs. The Etx pore also lacks a vestibule that is found in the α-hemolysin family of β-PFTs where the β-barrel begins close to the membrane spanning region (Supplementary Figure 7a, d, respectively). The Etx assembly measures ~120 Å across and ~98 Å in height. The lumen of the β-barrel measures ~24 Å (Cα-Cα) at its widest, although local restrictions are present (see below).

Each protomer in the pore structure can be divided into three domains (Figure 3a, b): the β-hairpin domain (blue), the cap domain (yellow) and the receptor binding domain (green). The β-hairpin domain (residues 95-173) creates the inner β-barrel, which begins at the top of the pore and runs through the entire length of the assembly, including the membrane-spanning region. The cap domain (residues 63-94, 174-198 and 235-260) at the extracellular side, also referred to as the collar[35], includes an outer β-barrel that surrounds the membrane-distal region of the inner β-barrel, and thus contributes to the highly conserved, concentric double β-barrel (DBB) fold, a common feature of the aβ-PFTs[41]. The receptor binding domain (residues 1-62 and 199-234) is unique to each β-PFT and determines the binding specificity of the toxin.

The β-hairpin domain

As has been shown previously[20], members of the aβ-PFTs form β-barrels that span the height of their pores. This domain includes the insertion loops that have been hypothesized to form the membrane spanning regions (Etx residues 123-148)[21, 42, 43]. As in lysenin, in fact the β-barrel recruits polypeptide from the flanking β-strands on either side of the insertion loop so that the β-hairpin domain actually comprises residues 95-173. The lumen of the pore is mostly lined with serine and threonine residues, yet another characteristic of the aerolysin family, but asparagine and glutamine residues are also present. Additionally, a number of salt bridges are present (Supplementary Figure 8c-e). Forming intra-chain bridges are Lys99-Asp168 and Lys108-Glu159. Lys130 with Glu137 form an inter-chain salt bridge which stabilizes the β-barrel near the intracellular side of the pore in addition to the hydrogen bonding network. The overall charge distribution in the lumen is therefore neutral (Supplementary Figure 9b). At its narrowest point the diameter of the lumen is constricted to ~12 Å by the seven Lys108 residues which protrude into the lumen (Supplementary Figure 8a and Supplementary Figure 9b, rectangle). The structure corroborates studies that show Etx has only a slight preference for anions[31, 32]. The β-turn at the intracellular side is formed by Thr132, Val133, Pro134 and Phe135. Aerolysin and Etx are conserved in this region. Pro134 is equivalent to Pro248 in aerolysin and, as in aerolysin, the β-turn main chain protrudes sideways, forming a rivet to anchor the barrel at the intracellular side (Figure 3c)[44].

The external surface of the Etx inner β-barrel reveals a number of interesting features (Figure 3c). In the intracellular side of the membrane two aromatic residues, Phe131 and Phe135, form the usual aromatic belt found in β-barrel transmembrane regions. However,

213 in the extracellular side of the membrane there are two aromatic belts. One is formed by
214 Tyr146 ~30 Å from the tip, and the other formed by His119 (H106 in Etx without
215 propeptide[45]) and Phe148 ~35 Å from the tip.
216
217 Examination of the unfiltered maps indicates that the detergent micelle density extends
218 above His119 and Phe148, suggesting these residues will be interacting with the
219 membrane (Supplementary Figure 10). Therefore, we propose that the membrane-
220 inserted region in the Etx pore comprises residues 119-148, close to the original
221 prediction[21]. Interestingly, histidine residues were also found in the detergent micelle
222 region of lysenin above the standard aromatic belt[20]. Towards the membrane-distal part
223 of the inner β-barrel, His162 (H149 in Etx without propeptide) is another important
224 residue for Etx activity[22, 45]. H162 (Nδ1) is within hydrogen bonding distance of D250
225 (Oδ2) which lies in the cap domain of the same chain (Figure 3d and Supplementary
226 Figure 8a).
227
228 **The receptor binding domain (RBD)**
229 This region undergoes minimal conformational changes in the transition from the water-
230 soluble form, as in lysenin[20]. Unique to Etx, and unlike lysenin and aerolysin, the
231 individual RBDs are well separated and do not interact with their neighbours (Figure 3b,
232 Supplementary Figure 7a-c), and thus do not contribute to any oligomerization surfaces.
233 The lack of physical constraints in the RBD could infer higher flexibility in receptor
234 selection and binding, and in part explains why the resolution of this domain is lower
235 than that of the other domains (Supplementary Figure 5). Overall, the RBD in the

oligomer overlaps well with the corresponding region of the crystal structure of Etx in its monomeric form (PDB ID: 1UYJ) (Supplementary Figure 11), with an RMSD of 1.7 Å (Cα- Cα). A number of tyrosine residues (Tyr 42, 43, 49 and 209; corresponding to Tyr 29, 30, 36 and 196 in[22, 46]) which were identified in earlier studies as important in receptor binding[22, 46] are located directly above the membrane in a position that would facilitate interaction with a receptor (Figure 3c). As shown in Supplementary Figure 9a, d, the tips of the RBD are predominantly hydrophobic.

The cap domain

The cap domain links the RBD to the β-hairpin domain and undergoes significant rearrangement in the pore form, as discussed below. In the pore conformation it contributes the outer β-barrel to the DBB fold (Figure 3d). In aerolysin, the DBB fold has been shown to be responsible for the SDS-resistant character of aerolysin[36]. In Etx the DBB fold is stabilised by hydrophobic interactions between the inner and outer β-barrel that includes valines, leucines, isoleucines, offset π-π stacking between Tyr84 and Phe105 residues, as well as some hydrogen bonds, including H162 and D250 mentioned above (Figure 3d and Supplementary Figure 8a, b).

To investigate the importance of the H162-D250 interaction, we constructed D250A and H162A mutants. Etx-H162A (corresponding to H149A in[45]) has previously been reported to have reduced, but not abolished, toxicity[45], and the crystal structure of P-Etx-H162A closely resembles that of wild type P-Etx[22], while purified recombinant Etx-D250A is completely inactive towards Super Dome cells, as shown in Supplementary Figure 12a,

259 and thermal stability assays indicate that P-Etx-D250A behaves similarly to wild type P-
260 Etx (Supplementary Figure 12b), suggesting that P-Etx-D250A is correctly folded.
261 Examination of D250 and H162 in the monomeric Etx crystal structure indicates that
262 D250 and H162 are not involved in any interactions, suggesting that the importance of
263 these residues lies in the H162-D250 hydrogen bond formed in the oligomer. SDS-PAGE
264 analysis of oligomer formation revealed that both Etx-D250A and Etx-H162A produce
265 SDS-resistant oligomers of the same apparent molecular weight as wild type Etx (~155
266 kDa, consistent with previous reports[2, 28, 29, 34]) (Supplementary Figure 13). When Super
267 Dome cells were incubated with activated wild type Etx, Etx-D250A or Etx-H162A
268 (Supplementary Figure 13a, lanes 11-13), oligomers were formed with a mean oligomer
269 yield of 5.09 ± 2.62% (S.E.M.) for Etx-D250A (Supplementary Figure 13b), albeit in a
270 concentration dependent manner (Supplementary Figure 14), and with a mean oligomer
271 yield of 44.54 ± 10.25% (S.E.M.) for Etx-H162A relative to wild type Etx
272 (Supplementary Figure 13b). These results suggest that while D250A oligomers
273 resembling the wild type ones, either in a pre-pore or post pre-pore state, can assemble,
274 they cannot produce pores that have a cytotoxic effect on cells (Supplementary Figure
275 12a), even at the highest concentration of 6 μM tested (2,426 times the CT_{50} dose of wild
276 type Etx). Further analysis of oligomer formation by native-PAGE revealed a much
277 larger complex of ~624 kDa relative to the SDS-resistant oligomers of ~155 kDa when
278 Super Dome cells were incubated with activated wild type Etx (Supplementary Figure 15,
279 lane 10). The same complex, albeit at lower intensity, was also observed when cells were
280 incubated with activated Etx-H162A (Supplementary Figure 15, lane 12), but was not
281 detectable when cells were incubated with activated Etx-D250A (Supplementary Figure

15, lane 11), providing further evidence that D250A oligomers detected by SDS-PAGE may not correspond to pores. Both D250A and H162A mutants retain their ability to bind to Super Dome cells (Supplementary Figure 13a, lanes 8-10, and Supplementary Figure 15a, lanes 7-9), suggesting that residues D250 and H162 are important for events downstream of receptor binding. Similar to activated wild type Etx, negative stain EM did not reveal regular particles other than elongated monomers and small clumps for activated Etx-D250A and Etx-H162A (Supplementary Figure 1).

Structural rearrangements during pore formation

Comparison of the crystal structure of Etx monomer to its membrane-inserted form illustrates the large conformational changes that occur upon pore formation (Figure 4 and Supplementary Movie 1). The cap domain moves downward towards the membrane by 45 Å creating a kink in the straight cap domain. In turn, the β-hairpin domain, consisting of the hypothetical insertion loop and the pre-insertion strands, as for lysenin[20], unfolds to create the inner β-barrel that spans the entire length of the Etx pore. In contrast to lysenin, the cap domain in Etx moves slightly away from the inner β-barrel rather than towards it.

To further understand how Etx assembles into an oligomer and the rearrangements required for transition to the pore state, we constructed a hypothetical pre-pore by superimposing the crystal structure monomer to the RBD of the pore structure and imposing 7-fold symmetry, similar to hypothetical pre-pores constructed previously for lysenin[20, 35]. This allowed us to observe some of the displacements that have to occur prior to pre-pore formation (Supplementary Figure 16). Calculations of molecular clashes

(inter-atom overlap >0.6 Å) highlight the potential regions that would have to rearrange upon oligomerisation. It is clear from these clashes that the CTP, as expected, severely obstructs oligomerization, and the pre-pore model illustrates why this region must be removed prior to monomer association. In addition to the CTP, other significant clashes occur near the oligomerisation surfaces on either side of a monomer, indicating again that some rearrangement will have to happen. Finally, the hypothetical insertion loop or tongue also creates clashes upon monomer association and, as described previously for lysenin[35], the displacement of the tongue region may be the driving force for the pre-insertion strands to unfold and the formation of the inner β-barrel.

Discussion

The pore form of Etx has long eluded structural determination, mostly owing to the difficulty of forming biologically active Etx oligomers in liposomes of various lipid compositions or detergent micelles without a receptor, which is unknown. Thus, the only viable way to study the pore form of Etx was to isolate the complexes directly from cells known to be susceptible to Etx. In this study, the use of Super Dome cells, reported to have 3 to 78-fold increased sensitivity to Etx relative to MDCK cells[39], combined with the use of increased concentration of DDM (2% (w/v)) relative to 0.05% (w/v) used in[34] maximized pore yield for subsequent purification, and thus were critical for structural determination of the Etx pore complex. Furthermore, due to the very small quantities of material that can be isolated from the membrane of cultured cells and the heterogeneity of the purified samples, cryo-EM technique was the only structural method that could be employed. Use of the VPP proved essential in our studies to achieve high resolution, owing to the challenging sample rather than its molecular mass (~225 kDa). First, particles could be identified by the automatic and manual picking procedures more efficiently, resulting in more particles (Supplementary Figure 4). Second, the overall quality of the data, as judged by B-factor estimation from both datasets, was higher for the VPP data, meaning we could achieve higher resolution than with the non-VPP data, given the number of particles (Supplementary Figure 6). While this manuscript was under review, another cryo-EM study of a relatively large complex (~500 kDa) also benefited by the use of the VPP[47], suggesting that VPP use could be advantageous for certain specimens which are not size limited. The resulting map at 3.2 Å resolution allowed an unambiguous model to be built for Etx pore.

A number of interesting mutants of Etx have been studied in the past whilst trying to understand how Etx transitions from the water-soluble to the pore form. Mutating H149 (H162 in our model) to alanine resulted in a significant decrease in activity of the recombinant toxin both in vitro and in vivo[45]. However, substitution with serine at position 162 does not abolish lethal activity[45], suggesting that H162A is less active not because of removal of the bulky imidazole side chain but possibly due to the loss of a hydrogen bond donor at this position. H162, located in the membrane-distal part of the inner β-barrel, has previously been equated to aerolysin Y221 and recent studies proposed that, similar to the aerolysin Y221G mutant, the Etx H162A mutant may prevent the β-hairpin domain involved in pore formation from unfolding[19, 41]. However, unlike the aerolysin Y221G mutant, the Etx H162A mutant did not reveal water-soluble, heptameric pre-pore particles by negative stain EM (Supplementary Figure 1b).

Examination of the Etx pore structure reveals that H162 may also play a role in stabilizing the DBB fold by forming a hydrogen bond with D250 in the cap domain. This interaction will stabilize the DBB fold further in addition to the hydrophobic interactions and make it more rigid. In agreement with this hypothesis, substitution of aspartate with alanine at position 250 results in a completely inactive Etx that displays ~95% reduction in SDS-resistant oligomers relative to wild type Etx. The reduced oligomerization of Etx-D250A and its complete inactivity towards Super Dome cells could be a result of either oligomer instability or a reduction in oligomer formation. Since D250 does not participate in any inter-chain interactions in the oligomer we cannot explain the latter.

The abolished cytotoxicity of Etx-D250A suggests that the SDS-resistant oligomers resembling the wild type ones may correspond to pre-pores or post pre-pores. This may explain why Etx-D250A oligomers resembling the wild type ones were not observed by native-PAGE immunoblot. Pre-pores or post pre-pores are expected to migrate differently to pores on native-PAGE as they will lack any associated detergents or lipids.

Further evidence for the importance of the DBB stability in pore formation also comes from previous mutagenesis studies. Tyrosine 84 in the cap domain and F105 in the inner β-barrel have previously been identified as important to Etx function[48]. Y84A completely abolishes pore formation and is only recoverable by substitution to another aromatic residue, whilst F105A has reduced cytotoxic activity towards MDCK cells at low toxin concentrations[48]. In the pore structure these two residues form a π-π stacking interaction (Figure 3d and Supplementary Figure 8b). Similar to D250A and H162A mutants, Y84A and F105A mutants also retain their ability to bind to MDCK cells.

Based on previous studies and the pore structure presented here, we propose that the stability of the DBB fold may be important in coupling the conformational changes that occur in the cap domain (the vertical collapse by 45 Å) to the insertion of the inner β-barrel into the membrane. By stabilizing the top end of the inner β-barrel as it is being formed by the unfolding of the β-hairpin domain, the insertion into the membrane will be analogous to a drill which is forced into the ground by applying force at the top. Similarly, the RBDs with their hydrophobic tips may keep the complex anchored to the membrane during membrane insertion, analogous to the stabilizing feet of the drill, by

384 either an interaction with the receptor or with the lipid bilayer itself. The pre-pore
385 structure of aerolysin by cryo-EM[36] showed that the DBB has already formed at this stage
386 and is a pre-requisite to insertion of the inner β-barrel into the membrane.
387
388 Monomeric P-Etx has previously been crystallized bound to β-OG in the PFM of the
389 carboxy-terminus[22]. In the pore form of Etx the β-OG binding site is disrupted and the
390 interacting residues (V85, F105 and T106, corresponding to V72, F92 and T93 in[22]) are
391 scattered amongst the inner β-barrel and the cap domain. Similar to aerolysin[49], in order
392 for Etx to cross the thick layer of glycocalyx covering the apical side of gut epithelial
393 cells, Etx may initially bind to surface oligosaccharides with low affinity, possibly
394 through the β-OG binding site at the carboxy-terminus, before being progressively
395 shuttled towards the membrane surface where it would bind with high affinity to its
396 receptor through the RBD at the amino-terminus. This hypothesis is supported by the
397 finding that polarized epithelial cells are more sensitive to Etx from their apical side,
398 which is more abundant in oligosaccharides, than from their basolateral side[29, 50]. Binding
399 of Etx to a double receptor in the nervous system has also been suggested previously[9].
400
401 The knowledge of conformational rearrangements and protomer interfaces established
402 upon pore formation can be applied to a traditional structure-based drug discovery
403 approach, in which high-affinity small compounds are identified that target structural
404 features to block pore formation, and thus impair bacterial virulence. Further studies on
405 Etx will have important implications for the development of novel therapeutics aimed at

406 the functional disruption of pore formation to prevent human and animal infections, and
407 are relevant for nano-biotechnology applications.
408

Methods

Materials

Chemicals were purchased from Sigma, UK, unless otherwise stated. The polyclonal antibody against Etx mutant Y30A-Y196A was raised in rabbits as described in[51]. After electrophoretic separation purified Etx pore was visualised by SimplyBlue staining (Invitrogen Ltd., Paisley, UK). Protein concentrations were determined using the Pierce™ BCA Protein Assay Kit (Fisher Scientific Ltd., Loughborough, UK). Synthetic oligonucleotides were sourced from Eurofins Genomics, Germany.

Recombinant protein production and purification

The gene, *etxB*, encoding epsilon protoxin (P-Etx) was PCR amplified using synthetic oligonucleotides Etx-*Nco*I-F and Etx-*Xho*I-R (Supplementary Table 1) designed to bear restriction enzyme sites *Nco*I and *Xho*I, respectively, to facilitate directional cloning into the expression vector pHis-Parallel1 (GenBank: AF097413.1). This fused the amino-terminal end of P-Etx without the 14 amino-terminal residues (KEISNTVSNEMSKK) to the 26 amino acid residue long peptide (MSYYHHHHHHDYDIPTTENLYFQGAM), which contains an amino-terminal polyhistidine (6 x His) affinity tag upstream of a spacer region (DYDIPTT) and the rTEV protease cleavage site (ENLYFQG). The fidelity of PCR amplification was verified by automated DNA sequencing (Eurofins Genomics, Germany). The recombinant plasmid expressing P-Etx is termed pHis-Parallel1-P-Etx. Amino acid numbering corresponds to P-Etx with the 13 amino acids amino-terminal peptide sequence, unless otherwise stated.

For expression of P-Etx, recombinant plasmid pHis-Parallel1-P-Etx was transformed into *E. coli* Rosetta 2 (DE3) cells (Merck, Darmstadt, Germany) and expression of P-Etx was induced using the autoinduction system as described before[22] but with modifications. In brief, cells (100 ml) were grown at ACDP/ACGM containment level 3 in ZYM-5052 autoinducing medium supplemented with 50 μg ml^{-1} carbenicillin and 34 μg ml^{-1} chloramphenicol and cultured at 37 ˚C for 3 h at 300 rpm, then for a further 24 h at 20 ˚C, 300 rpm. Cells were harvested by centrifugation at 10,000 *g* for 10 min at 4 °C and the cell pellet was lysed by 10 ml BugBuster™ Protein Extraction Reagent (Merck, Darmstadt, Germany) containing rlysozyme™ (0.5 μl at 30 KU μl^{-1}) (Merck, Darmstadt, Germany) and Benzonase® Nuclease (10 μl at 25 U μl^{-1}) (Merck, Darmstadt, Germany). The cell suspension was incubated on a rotating mixer for 25 min at room temperature and centrifuged at 16,000 *g* for 20 min at 4 °C to separate soluble and insoluble fractions. The supernatant was loaded onto His GraviTrap columns (GE Healthcare Life Sciences, Little Chalfont, UK) following the manufacturer's guidelines. In brief, His-tagged P-Etx was bound to the affinity column using a buffer composed of 20 mM sodium phosphate, 500 mM NaCl, 20 mM imidazole, pH 7.4. The column was washed with a buffer composed of 20 mM sodium phosphate, 500 mM NaCl, 60 mM imidazole, pH 7.4. Recombinant P-Etx was eluted in a buffer composed of 20 mM sodium phosphate, 500 mM NaCl, 500 mM imidazole, pH 7.4. All purification steps were carried out at 4 °C. For buffer exchange and sample clean-up, P-Etx-containing eluate was applied to a PD-10 Desalting Column (GE Healthcare Life Sciences, Little Chalfont, UK) and eluted in Dulbecco's phosphate-buffered saline (DPBS) pH 7.0 - 7.2 (Invitrogen). Protein concentrations were determined by BCA assay.

455

456 **Activation of P-Etx by trypsin**

457 Purified recombinant P-Etx was activated with trypsin, TPCK treated from bovine
458 pancreas, which removes the carboxy-terminal peptide (CTP) sequence. Trypsin was
459 prepared in DPBS and added to recombinant P-Etx at 1:100 (w/w) ratio and incubated at
460 room temperature for 1 h. The reaction was stopped by adding trypsin inhibitor (0.66 mg
461 per 1 mg trypsin) to the digest. Removal of the CTP sequence was assessed by SDS-
462 polyacrylamide gel electrophoresis (PAGE).

463

464 **Site directed mutagenesis**

465 Mutation D250A or H162A was introduced into wild type recombinant Etx using primer
466 pairs D250A-F and D250A-R or H162A-F and H162A-R, respectively (Supplementary
467 Table 1) and the QuickChange Lightning Site-Directed Mutagenesis Kit (Agilent
468 Technologies, Inc. Santa Clara, US) according to the manufacturer's instructions. The
469 presence of the intended mutation was verified by automated DNA sequencing (Eurofins
470 Genomics, Germany).

471

472 **Thermostability assay**

473 Thermostability of purified recombinant P-Etx-D250A was assessed by mixing purified
474 protein (0.25 mg ml^{-1}) with 240x SYPRO Orange protein gel stain. Fluorescence was
475 monitored using a QuantStudio™ 6 Real-Time PCR System (Applied Biosystems, USA)
476 with a 1% thermal gradient from 25 °C to 99 °C. The fluorescence data obtained was

477 analysed using the Protein Thermal Shift Software (Applied Biosystems, USA) to
478 calculate the melting temperature (Tm) using the Boltzmann method.
479
480 **Cell culture**
481 Super Dome (ATCC® CRL-2286™; American Type Culture Collection (ATCC), USA)
482 cells, a canine epithelial-like cell line established by cloning from the MDCK (ATCC®
483 CCL-34™) cell line, were routinely cultured in Dulbecco's Modified Eagle's Medium /
484 Ham's F-12 medium (DMEM/F-12, HEPES; Life Technologies) with 2.5 mM L-
485 glutamine, 15 mM HEPES, 0.5 mM sodium pyruvate and 1.2 g l^{-1} sodium bicarbonate
486 supplemented with 0.05 mM nonessential amino acids and 10% Foetal Bovine Serum
487 Gold (PAA, Pasching, Austria) at 37 °C in a humidified atmosphere of 95% air/5% CO_2.
488 The culture medium was replaced every 2 to 3 days. Cells were routinely detached by
489 incubation in trypsin/EDTA and split as appropriate (typically 1:5 dilutions). For dome
490 formation, Super Dome cells were fed twice a day by a complete medium change.
491
492 **Cytotoxicity assay**
493 The cytotoxic activity of trypsin-activated Etx toward Super Dome cells was determined
494 by measuring the amount of LDH released from the cytosol of lysed cells into the cell
495 culture medium using the CytoTox 96 nonradioactive cytotoxicity assay kit (Promega,
496 Southampton, UK) according to the manufacturer's protocol. In brief, a two-fold dilution
497 series of each activated toxin (ranging from 139 nM to 0.067 nM) was prepared in DPBS
498 and added to cells seeded into 96-well plates (3 x 10^4 cells per well). Following
499 incubation at 37 °C for 3 h, cell culture medium (50 µl) was harvested from cell

monolayers, transferred to a fresh 96-well enzymatic assay plate and 50 µl of reconstituted substrate mix was added to each well. The plate was incubated for 30 min at room temperature, protected from light. Absorbance was measured at 490 nm using a Tecan Infinite 200 PRO Microplate Reader (Tecan Group Ltd., Switzerland). The absorbance values for each sample were normalized by subtracting the absorbance value obtained for the culture medium from untreated cells. The toxin dose required to kill 50% of the cell monolayer (CT_{50}) was determined by nonlinear regression analysis, fitting a variable slope log(dose) versus response curve, constraining F to a value of 50 ($logCT_{50}$ = logCTF - (1/HillSlope)*log(F/(100-F)).

Epsilon toxin pore assembly

Super Dome cells were grown to confluency in 30 times T175 flasks. Each flask of cells was incubated with 5 ml cell culture medium containing trypsin-activated Etx (25 µg ml^{-1}; 50 times the average minimum dose required to lyse 100% cells) at 37 °C for 1 h to allow binding and pore formation. Lysed cells were centrifuged at 1,500 *g* for 15 min at 4 °C to pellet cellular debris and unbound Etx was removed by ultracentrifugation at 100,000 *g* for 1 h at 4 °C using a Beckman Type 70Ti rotor. Solubilisation of toxin complex from Super Dome cells was carried out by resuspending the pellet in DPBS (pH 7.0 – 7.2) containing 137 mM NaCl and 2% (w/v) n-dodecyl-β-D-maltoside (DDM) and incubation at 4 °C overnight, a modification of the method described by Shimada *et al*.[34] where the toxin complex from MDCK cells was solubilized by resuspending the pellet in 20 mM sodium phosphate buffer (pH 7.4) containing 0.05% (w/v) DDM and incubation at 25 °C for 1 h. After incubation, insoluble material was removed by ultracentrifugation

523 at 75,000 *g* for 45 min at 10 °C using a Beckman Type 70Ti rotor. Solubilised Etx
524 oligomers were bound to Ni-NTA Agarose resin (Qiagen), washed with two times 20
525 volumes of DPBS, 0.02% (w/v) DDM, and eluted in three volumes of DPBS, 200 mM
526 imidazole, 0.02% (w/v) DDM.
527
528 **Detergent screening**
529 To screen for a suitable detergent that could efficiently extract and maintain Etx pores
530 soluble, Super Dome cell membrane was incubated with trypsin-activated Etx for 1 h at
531 37 °C and membrane incubations were distributed between nine tubes. After
532 ultracentrifugation at 100,000 *g* for 1 h at 4 °C using a TLA 120.1 rotor, each pellet was
533 resuspended in DPBS containing 137 mM NaCl and detergent (1% (w/v) DDM, 1%
534 (w/v) DM, 0.5% (w/v) C12E8, 1% (w/v) FC-12, 2% (w/v) β-OG, 2% (w/v) C8E4, 1%
535 (w/v) CYMAL-5, 1% (w/v) LDAO or 1% (w/v) LMNG) and incubated overnight at 4 °C
536 with occasional shaking. After incubation, 10 µl aliquots were removed from each tube
537 for Western blot analysis (total protein in detergent) and insoluble material was removed
538 by ultracentrifugation, as before. The supernatants, which contained solubilised Etx pore,
539 were collected and 10 µl aliquots were removed from each tube to assess Etx pore
540 solubilisation by Western blot analysis using 6×-His Tag Monoclonal Antibody
541 (4A12E4) (Invitrogen, Paisley, UK; catalogue number 37-2900) and IRDye® 800CW
542 Goat (polyclonal) Anti-Mouse IgG (H+L), Highly Cross Adsorbed secondary antibody
543 (LI-COR Biosciences, Lincoln, USA; catalogue number 926-32210) at 1:500 and 1:5,000
544 dilutions, respectively. The solubilization yields for each detergent were determined by

545 calculating the % of Etx pore in the supernatant relative to its amount in the total protein
546 sample using Image Studio ver 5.2 software (LI-COR Biosciences, Lincoln, USA).
547
548 **Epsilon pore purification**
549 For DDM-extracted samples, solubilised Etx oligomers were bound to Ni-NTA resin
550 (Qiagen), washed with 20 volumes of DPBS containing 20 mM imidazole and 0.02%
551 (w/v) DDM, transferred to a BioRad gravity-flow column, washed again with 20 volumes
552 of DPBS containing 20 mM imidazole and 0.02% (w/v) DDM, and eluted in three
553 volumes of DPBS containing 200 mM imidazole and 0.02% (w/v) DDM.
554
555 **Binding and oligomerization**
556 Super Dome cells were grown to confluence in 6-well plates (1.2×10^6 cells per well) and
557 after washing cells three times with DPBS to remove residual trypsin, each well was
558 incubated with 2 ml pre-warmed DMEM-F12 medium containing trypsin-activated
559 recombinant Etx wild type, Etx-D250A or Etx-H162A (391 ng ml^{-1}, equivalent to 5x
560 CT_{50} dose of wild type Etx) at 37 °C for 1 h to allow binding and/or oligomerisation.
561 Cells were subsequently washed three times with DPBS to remove unbound Etx, lysed by
562 three cycles of freezing and thawing in 100 µl DPBS supplemented with Halt™ Protease
563 Inhibitor Cocktail (100×) (Thermo Fisher Scientific, UK) at a final concentration of 1x,
564 and harvested by scraping. The collected cells were transferred to a microcentrifuge tube
565 and solubilized in DPBS containing 1% (w/v) DDM by incubation at 4 °C overnight with
566 occasional shaking. After incubation, insoluble material was removed by centrifugation at

567 20,000 *g* for 30 min at 4 °C and the concentration of solubilised protein was determined
568 by BCA assay.
569
570 Toxin complexes or monomers in solubilisation buffer were analysed by native-PAGE
571 and SDS-PAGE. Solubilized proteins were resolved by NuPAGE™ 7% Tris-Acetate
572 Protein Gels (Invitrogen Ltd., Paisley, UK) using Surelock Xcell apparatus (Invitrogen
573 Ltd., Paisley, UK). For protein gel electrophoresis under denaturing running conditions
574 NuPAGE™ Tris-Acetate SDS Running Buffer (Invitrogen Ltd., Paisley, UK) and
575 NuPAGE LDS sample buffer (Invitrogen Ltd., Paisley, UK) were used. For protein gel
576 electrophoresis under native running conditions Novex™ Tris-Glycine Native Running
577 Buffer (Invitrogen Ltd., Paisley, UK) and Novex™ Tris-Glycine Native Sample Buffer
578 (Invitrogen Ltd., Paisley, UK) were used. Denaturing gels were electrophoresed at 150 V
579 for 1 h at room temperature, while native gels were electrophoresed at 150V for 2 h in ice
580 cold running buffer. For SDS-PAGE the molecular weight standard Perfect Protein™
581 Marker, 10 to 225 kDa (Merck, Darmstadt, Germany) was used. For native-PAGE the
582 molecular weight marker NativeMark™ Unstained Protein Standard (Invitrogen Ltd.,
583 Paisley, UK) was used.
584
585 After electrophoresis, proteins in the gel were transferred to a nitrocellulose membrane
586 using the Trans-Blot® Turbo™ Transfer System (Bio-Rad). The membrane was blocked
587 with PBS containing 0.1% Tween-20 and 5% skim milk and bound P-Etx and/or
588 oligomeric complexes were detected with rabbit anti-Etx polyclonal primary antibody[51] at
589 1:500 dilution and IRDye® 800CW goat anti-rabbit IgG (H + L) secondary antibody (LI-

COR Biosciences, Lincoln, USA; catalogue number 926-32211) at 1:5,000 dilution. For loading control the mouse monoclonal Na^+/K^+-ATPase α1 (C464.6): sc-21712 primary antibody (Santa Cruz Biotechnology; catalogue number sc-21712) and the IRDye® 680RD goat (polyclonal) anti-mouse IgG (H+L) secondary antibody (LI-COR Biosciences, Lincoln, USA; catalogue number 925-68070) were used at 1:200 and 1:5,000 dilutions, respectively. Antibodies were diluted in PBS containing 0.1% Tween-20 and 3% skim milk. Immuno-reactive bands were detected using the Odyssey CLx infrared imaging system (LI-COR Biosciences, Lincoln, USA). Quantitative analyses were performed using the Image Studio ver 5.2 software and the Housekeeping Protein Normalization Protocol (LI-COR Biosciences, Lincoln, USA). The oligomer yield for each Etx variant was determined by calculating the percentage of fluorescence intensity relative to wild type toxin.

Negative stain electron microscopy

Purified recombinant P-Etx variants were trypsin-activated as described above. After activation, samples were diluted to 0.02 mg ml^{-1} and 3 µl was added to freshly glow-discharged carbon-coated grids for 60 seconds before staining with 20 µl of 2% (w/v) aqueous uranyl acetate. Grids were then imaged on a Philips CM200 FEG transmission electron microscope operating at an accelerating voltage of 200 kV. Images were recorded at a calibrated pixel size of 2 Å on a TVIPS F224HD CCD camera.

Specimen preparation and data collection

612 Etx eluate fraction 4 (approximately 0.04 mg ml^{-1}) was diluted three-fold in elution buffer
613 (DPBS containing 20 mM imidazole and 0.02% (w/v) DDM) and deposited on Quantifoil
614 R1.2/1.3 grids overlaid with graphene oxide, as described in[20]. Grids were then blotted
615 and plunge-frozen using a custom-made device and stored in LN2 until further use. Data
616 was collected on a FEI Titan Krios operating at an accelerating voltage of 300 kV. All
617 datasets were collected on a FEI Falcon 3EC direct electron detector at a nominal
618 magnification of 75K× (calibrated pixel size of 1.07 Å) and a dose rate of 0.6e- per pixel
619 per second in counting mode over 60 seconds and 75 fractions. Conventionally defocused
620 and phase plate datasets were collected using the EPU software (Thermo-Fisher
621 Scientific). In brief, grid squares and suitable holes were selected and microscope
622 alignments were performed. Just prior to data collection, the phase plate was inserted and
623 the un-scattered beam was made parallel by observing the Ronchigram in the back focal
624 plane of the objective lens over an empty specimen area. Condenser astigmatism was
625 corrected by reducing the smearing of the Ronchigram near the blow-up point. Due to the
626 extremely low screen current used (~0.014 nA), the 150 µm C2 aperture was used to aid
627 in this process and then switched back to the 50 µm aperture. Coma and astigmatism
628 were corrected using AutoCTF. Defocused data were collected by defocusing between -2
629 µm and -3.5 µm every 15 µm, and phase plate data between -0.3 and -0.8 µm with
630 focusing at every hole.
631
632 **Image processing**
633 All data datasets were processed in Relion-3[52]. Micrographs were first corrected for large
634 movements using MotionCorr2[53] and a 4 x 4 patch with no grouping. CTF parameters

were estimated using GTCF[54]. Autopicking was performed in Relion after creating references from manually picked particles. The processing procedure is summarized in Supplementary Figure 4. The resolution was calculated using Gold-Standard 0.143 criterion, resulting in a 4.6 Å map for the defocused dataset and 3.2 Å for the phase plate dataset. The variation in resolution in the map was calculated using the Relion local resolution implementation. Box sizes of 220 pixels were used for both the defocused and phase plate datasets. To ensure that high resolution information was not lost by the high defocus values used for the former dataset, particles were re-extracted in 400 pixel boxes and subjected to 3D refinement. No increase in resolution was observed for the larger box size particles. B-factor plots were calculated using the bfactor_plot.py scripts provided with Relion.

Model building and refinement

A model was built into the 3.2 Å map by initially docking the receptor binding domain of wild type Etx crystal structure (PDB: 1UYJ) and then extending this using Coot. Refinement of the atomic coordinates was performed using Phenix[55] real space refine and re-iterating the model building-refinement procedure several times.

Statistics

Data were analyzed using Prism v7 software (GraphPad Software, Inc., La Jolla, CA, USA). Data are expressed as the mean value ± SEM.

Data availability

Data supporting the findings of this manuscript are available from the corresponding author upon reasonable request. A reporting summary for this Article is available as a Supplementary Information file.

The cryo-EM maps of epsilon toxin pore have been deposited to the Electron Microscopy Data Bank under accession number EMD-4789 and the refined atomic coordinates have been deposited to the Protein Data Bank under accession number 6RB9. The source data for Figure 1 and Supplementary Figures 2, 12-15 are provided as a Source Data file.

References

1. Rumah KR, Linden J, Fischetti VA, Vartanian T. Isolation of *Clostridium perfringens* type B in an individual at first clinical presentation of multiple sclerosis provides clues for environmental triggers of the disease. *PLoS One* **8**, e76359 (2013).

2. Rumah KR*, et al.* The Myelin and Lymphocyte Protein MAL Is Required for Binding and Activity of *Clostridium perfringens* epsilon-Toxin. *PLoS Pathog* **11**, e1004896 (2015).

3. Wagley S*, et al.* Evidence of *Clostridium perfringens* epsilon toxin associated with multiple sclerosis. *Mult Scler*, 1352458518767327 (2018).

4. Habeeb AF. Studies on epsilon-prototoxin of *Clostridium perfringens* type D. Physicochemical and chemical properties of epsilon-prototoxin. *Biochim Biophys Acta* **412**, 62-69 (1975).

5. Minami J, Katayama S, Matsushita O, Matsushita C, Okabe A. Lambda-toxin of *Clostridium perfringens* activates the precursor of epsilon-toxin by releasing its N- and C-terminal peptides. *Microbiol Immunol* **41**, 527-535 (1997).

6. Miyata S, Matsushita O, Minami J, Katayama S, Shimamoto S, Okabe A. Cleavage of a C-terminal peptide is essential for heptamerization of *Clostridium perfringens* epsilon-toxin in the synaptosomal membrane. *J Biol Chem* **276**, 13778-13783 (2001).

7. Worthington RW, Mulders MS. Physical changes in the epsilon prototoxin molecule of *Clostridium perfringens* during enzymatic activation. *Infect Immun* **18**, 549-551 (1977).

8. Nagahama M, Sakurai J. Distribution of labeled *Clostridium perfringens* epsilon toxin in mice. *Toxicon* **29**, 211-217 (1991).

9. Wioland L, Dupont JL, Bossu JL, Popoff MR, Poulain B. Attack of the nervous system by *Clostridium perfringens* Epsilon toxin: from disease to mode of action on neural cells. *Toxicon* **75**, 122-135 (2013).

10. Podobnik M, Kisovec M, Anderluh G. Molecular mechanism of pore formation by aerolysin-like proteins. *Philos Trans R Soc Lond B Biol Sci* **372**, (2017).

11. Szczesny P, Iacovache I, Muszewska A, Ginalski K, van der Goot FG, Grynberg M. Extending the aerolysin family: from bacteria to vertebrates. *PLoS One* **6**, e20349 (2011).

12. Janda JM, Abbott SL. Evolving concepts regarding the genus *Aeromonas*: an expanding panorama of species, disease presentations, and unanswered questions. *Clin Infect Dis* **27**, 332-344 (1998).

13. Briggs DC*, et al.* Structure of the food-poisoning *Clostridium perfringens* enterotoxin reveals similarity to the aerolysin-like pore-forming toxins. *J Mol Biol* **413**, 138-149 (2011).

14. Ballard J, Crabtree J, Roe BA, Tweten RK. The primary structure of *Clostridium septicum* alpha-toxin exhibits similarity with that of *Aeromonas hydrophila* aerolysin. *Infect Immun* **63**, 340-344 (1995).

15. Leone P*, et al.* X-ray and Cryo-electron Microscopy Structures of Monalysin Pore-forming Toxin Reveal Multimerization of the Pro-form. *J Biol Chem* **290**, 13191-13201 (2015).

16. Shogomori H, Kobayashi T. Lysenin: a sphingomyelin specific pore-forming toxin. *Biochim Biophys Acta* **1780**, 612-618 (2008).

17. Sher D*, et al.* Hydralysins, a new category of β-pore-forming toxins in cnidaria. *J Biol Chem* **280**, 22847-22855 (2005).

18. Akiba T*, et al.* Crystal structure of the parasporin-2 *Bacillus thuringiensis* toxin that recognizes cancer cells. *J Mol Biol* **386**, 121-133 (2009).

19. Degiacomi MT*, et al.* Molecular assembly of the aerolysin pore reveals a swirling membrane-insertion mechanism. *Nat Chem Biol* **9**, 623-629 (2013).

20. Bokori-Brown M, Martin TG, Naylor CE, Basak AK, Titball RW, Savva CG. Cryo-EM structure of lysenin pore elucidates membrane insertion by an aerolysin family protein. *Nat Commun* **7**, 11293 (2016).

21. Cole AR, Gibert M, Popoff M, Moss DS, Titball RW, Basak AK. *Clostridium perfringens* epsilon-toxin shows structural similarity to the pore-forming toxin aerolysin. *Nat Struct Mol Biol* **11**, 797-798 (2004).

22. Bokori-Brown M*, et al. Clostridium perfringens* epsilon toxin H149A mutant as a platform for receptor binding studies. *Protein Sci* **22**, 650-659 (2013).

23. Fennessey CM, Ivie SE, McClain MS. Coenzyme depletion by members of the aerolysin family of pore-forming toxins leads to diminished ATP levels and cell death. *Mol Biosyst* **8**, 2097-2105 (2012).

24. Gill DM. Bacterial toxins: a table of lethal amounts. *Microbiol Rev* **46**, 86-94 (1982).

25. Mantis NJ. Vaccines against the category B toxins: Staphylococcal enterotoxin B, epsilon toxin and ricin. *Adv Drug Deliv Rev* **57**, 1424-1439 (2005).

26. Lindsay CD. Assessment of aspects of the toxicity of *Clostridium perfringens* epsilon-toxin using the MDCK cell line. *Hum Exp Toxicol* **15**, 904-908 (1996).

27. Lindsay CD, Hambrook JL, Upshall DG. Examination of toxicity of *Clostridium perfringens* -toxin in the MDCK cell line. *Toxicol In Vitro* **9**, 213-218 (1995).

28. Nagahama M, Ochi S, Sakurai J. Assembly of *Clostridium perfringens* epsilon-toxin on MDCK cell membrane. *J Nat Toxins* **7**, 291-302 (1998).

29. Petit L, Gibert M, Gillet D, Laurent-Winter C, Boquet P, Popoff MR. *Clostridium perfringens* epsilon-toxin acts on MDCK cells by forming a large membrane complex. *J Bacteriol* **179**, 6480-6487 (1997).

30. Nagahama M, Hara H, Fernandez-Miyakawa M, Itohayashi Y, Sakurai J. Oligomerization of *Clostridium perfringens* epsilon-toxin is dependent upon membrane fluidity in liposomes. *Biochemistry* **45**, 296-302 (2006).

31. Nestorovich EM, Karginov VA, Bezrukov SM. Polymer partitioning and ion selectivity suggest asymmetrical shape for the membrane pore formed by epsilon toxin. *Biophys J* **99**, 782-789 (2010).

32. Petit L, Maier E, Gibert M, Popoff MR, Benz R. *Clostridium perfringens* epsilon toxin induces a rapid change of cell membrane permeability to ions and forms channels in artificial lipid bilayers. *J Biol Chem* **276**, 15736-15740 (2001).

33. Robertson SL, Li J, Uzal FA, McClane BA. Evidence for a prepore stage in the action of *Clostridium perfringens* epsilon toxin. *PLoS One* **6**, e22053 (2011).

34. Shimada H, Kitada S. Mega assemblages of oligomeric aerolysin-like toxins stabilized by toxin-associating membrane proteins. *J Biochem* **149**, 103-115 (2011).

35. Podobnik M*, et al.* Crystal structure of an invertebrate cytolysin pore reveals unique properties and mechanism of assembly. *Nat Commun* **7**, 11598 (2016).

36. Iacovache I, De Carlo S, Cirauqui N, Dal Peraro M, van der Goot FG, Zuber B. Cryo-EM structure of aerolysin variants reveals a novel protein fold and the pore-formation process. *Nat Commun* **7**, 12062 (2016).

37. Moniatte M, van der Goot FG, Buckley JT, Pattus F, van Dorsselaer A. Characterisation of the heptameric pore-forming complex of the *Aeromonas* toxin aerolysin using MALDI-TOF mass spectrometry. *FEBS Lett* **384**, 269-272 (1996).

38. Tsitrin Y*, et al.* Conversion of a transmembrane to a water-soluble protein complex by a single point mutation. *Nat Struct Biol* **9**, 729-733 (2002).

39. Boley M, Langenbach, K, Beck, B. Rapid identification of cell lines sensitive to *Clostridium perfringens* epsilon toxin. (eds). American Type Culture Collection (2010).

40. Danev R, Baumeister W. Cryo-EM single particle analysis with the Volta phase plate. *Elife* **5**, (2016).

41. Cirauqui N, Abriata LA, van der Goot FG, Dal Peraro M. Structural, physicochemical and dynamic features conserved within the aerolysin pore-forming toxin family. *Sci Rep* **7**, 13932 (2017).

42. Bokori-Brown M, Savva CG, Fernandes da Costa SP, Naylor CE, Basak AK, Titball RW. Molecular basis of toxicity of *Clostridium perfringens* epsilon toxin. *FEBS J* **278**, 4589-4601 (2011).

43. Knapp O, Maier E, Benz R, Geny B, Popoff MR. Identification of the channel-forming domain of *Clostridium perfringens* Epsilon-toxin (ETX). *Biochim Biophys Acta* **1788**, 2584-2593 (2009).

44. Iacovache I*, et al.* A rivet model for channel formation by aerolysin-like pore-forming toxins. *EMBO J* **25**, 457-466 (2006).

45. Oyston PC, Payne DW, Havard HL, Williamson ED, Titball RW. Production of a non-toxic site-directed mutant of *Clostridium perfringens* epsilon-toxin which induces protective immunity in mice. *Microbiology* **144 (Pt 2)**, 333-341 (1998).

46. Ivie SE, McClain MS. Identification of amino acids important for binding of *Clostridium perfringens* epsilon toxin to host cells and to HAVCR1. *Biochemistry* **51**, 7588-7595 (2012).

47. Greber BJ, Toso DB, Fang J, Nogales E. The complete structure of the human TFIIH core complex. *Elife* **8**, (2019).

48. Jiang Z, Chang J, Wang F, Yu L. Identification of tyrosine 71 as a critical residue for the cytotoxic activity of *Clostridium perfringens* epsilon toxin towards MDCK cells. *J Microbiol* **53**, 141-146 (2015).

49. Abrami L, Fivaz M, Glauser PE, Sugimoto N, Zurzolo C, van der Goot FG. Sensitivity of polarized epithelial cells to the pore-forming toxin aerolysin. *Infect Immun* **71**, 739-746 (2003).

50. Petit L, Gibert M, Gourch A, Bens M, Vandewalle A, Popoff MR. *Clostridium perfringens* epsilon toxin rapidly decreases membrane barrier permeability of polarized MDCK cells. *Cell Microbiol* **5**, 155-164 (2003).

51. Bokori-Brown M*, et al. Clostridium perfringens* epsilon toxin mutant Y30A-Y196A as a recombinant vaccine candidate against enterotoxemia. *Vaccine* **32**, 2682-2687 (2014).

52. Zivanov J*, et al.* New tools for automated high-resolution cryo-EM structure determination in RELION-3. *Elife* **7**, (2018).

53. Zheng SQ, Palovcak E, Armache JP, Verba KA, Cheng Y, Agard DA. MotionCor2: anisotropic correction of beam-induced motion for improved cryo-electron microscopy. *Nat Methods* **14**, 331-332 (2017).

54. Zhang K. Gctf: Real-time CTF determination and correction. *J Struct Biol* **193**, 1-12 (2016).

55. Afonine PV*, et al.* Real-space refinement in PHENIX for cryo-EM and crystallography. *Acta Crystallogr D Struct Biol* **74**, 531-544 (2018).

Acknowledgements

We thank Professor Nicholas Harmer and Alice Cross, University of Exeter, UK for assistance with the thermostability assay. We also wish to thank Dr Shaoxia Chen, Dr Giuseppe Cannone, Dr Greg McMullan, MRC Laboratory of Molecular Biology, Cambridge, UK; Dr Peter Moody, University of Leicester, UK; and Dr Edmund Kunji, MRC Mitochondrial Biology Unit, Cambridge, UK for helpful discussions and advice. This work was supported by grants from the UK Medical Research Council (MC-A021-53019) and the Wellcome Trust (WT089618MA).

Author Contributions

C.G.S. collected the cryo-EM data, performed the image processing and model building, analysed the data and wrote the paper. A.R.C contributed to model building, analysed the data and wrote the paper. C.E.N. M.R.P., D.S.M, A.K.B. and R.W.T. analysed the data and wrote the paper. M.B.-B. purified proteins, assembled and purified the pore complex, conducted the cytotoxicity, thermostability and oligomerisation assays, generated D250A site directed mutant, developed experimental methods, analysed the data, wrote the paper and coordinated the study. D.S.M, A.K.B and R.W.T initiated the project.

Competing Interests

The authors declare no competing interests.

Figure legends

Figure 1 Cytotoxic activity of wild type epsilon toxin towards Super Dome cells

(**a**) The cytotoxic activity of trypsin-activated recombinant wild type Etx towards Super Dome cells was determined by measuring the release of LDH from lysed cells. Results were normalised to the signal from cells treated with DPBS only (0% lysis) and cells treated with 0.9% (v/v) Triton X-100 (100% lysis). Results are presented as the mean of triplicate assays, each performed in triplicate (± S.E.M.). (**b**) Purified Etx pore was separated by SDS-PAGE and visualized by Coomassie staining. Arrows indicate the positions of Etx pore (p) and Etx monomer (m). Source data are provided as a Source Data file.

Figure 2 Cryo-EM of epsilon toxin pores using the Volta phase plate

(**a**) Electron micrograph of a typical field of view of isolated Etx pores. Particles that were included in the final 3D map are highlighted. (**b**) Characteristic 2D class averages. Sharpened cryo-EM map of the pore colored by monomer as visualized from the side (**c**) and extracellular (**d**) views. Scale bar corresponds to 50 nm.

Figure 3 Atomic model of the epsilon toxin pore

Cartoon representation of the heptameric Etx model with height, width and lumen dimensions indicated (**a, b**). The monomers are coloured by domain; green - receptor binding domain, blue - β hairpin domain, yellow - cap domain. (**c**) Close-up view of the inner β-barrel and membrane spanning region. Residues identified in previous studies as important to receptor binding in the RBD, as well as residues forming the aromatic belts,

are highlighted in stick representation. The approximate boundaries of the lipid bilayer are coloured light brown. (**d**) Close-up view of the DBB fold viewed from the membrane side with interacting residues shown in stick representation.

Figure 4 Conformational changes accompanying pore formation

Wire representation of Etx monomers in the water-soluble and membrane-inserted state coloured by domain as in Figure 3 and viewed from different angles (**a-c**). The two models were superimposed by their RBD which remains mostly unchanged during the transition. The cap domain collapses by 45 Å allowing the pre-insertion strands to get closer to the membrane and form the inner β-barrel. The heptameric pore is also shown for context. Curved arrow in (**c**) illustrates outward movement of the cap domain in the membrane-inserted form.

a

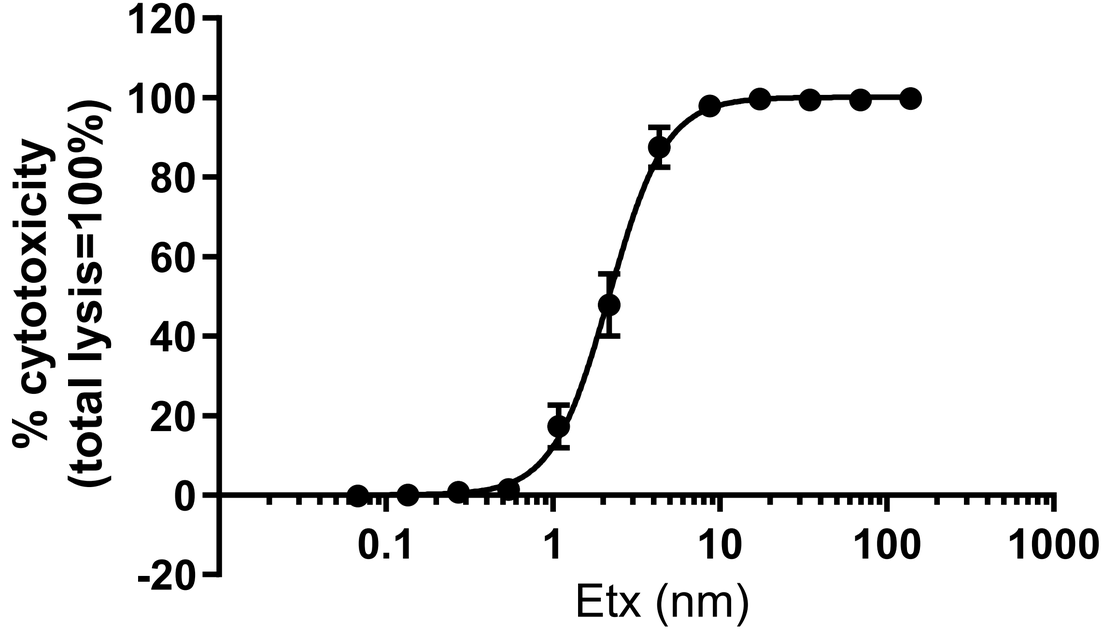
% cytotoxicity
(total lysis=100%)
120
100
80
60
40
20
0
-20
0.1
1
10
100
1000
Etx (nm)

b

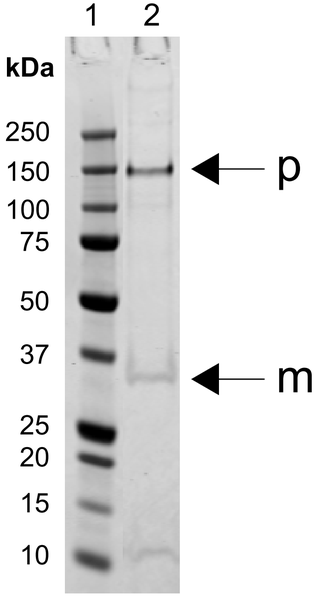
1
2
kDa
250
150
100
75
50
37
25
20
15
10
p
m

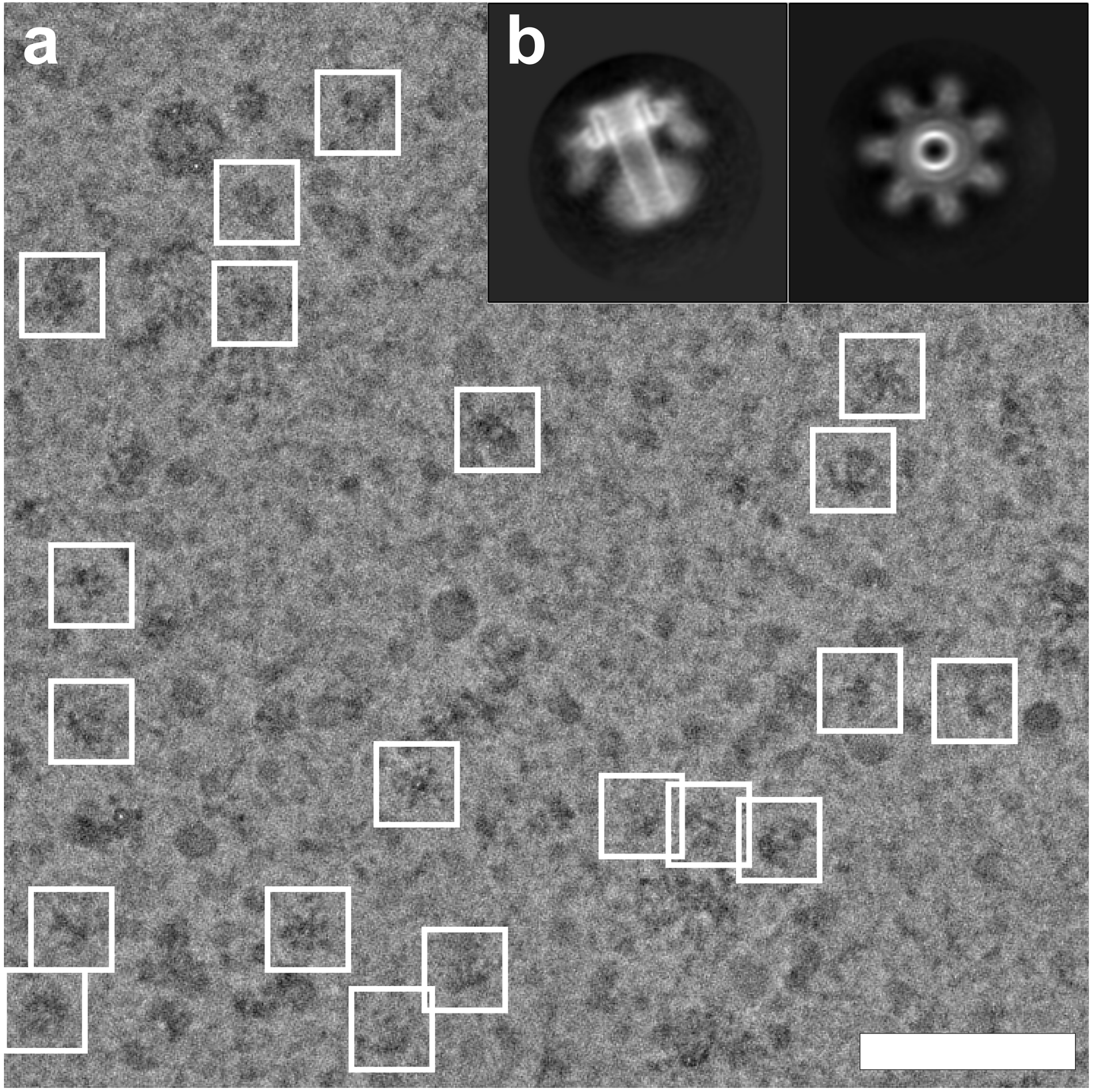
a

b

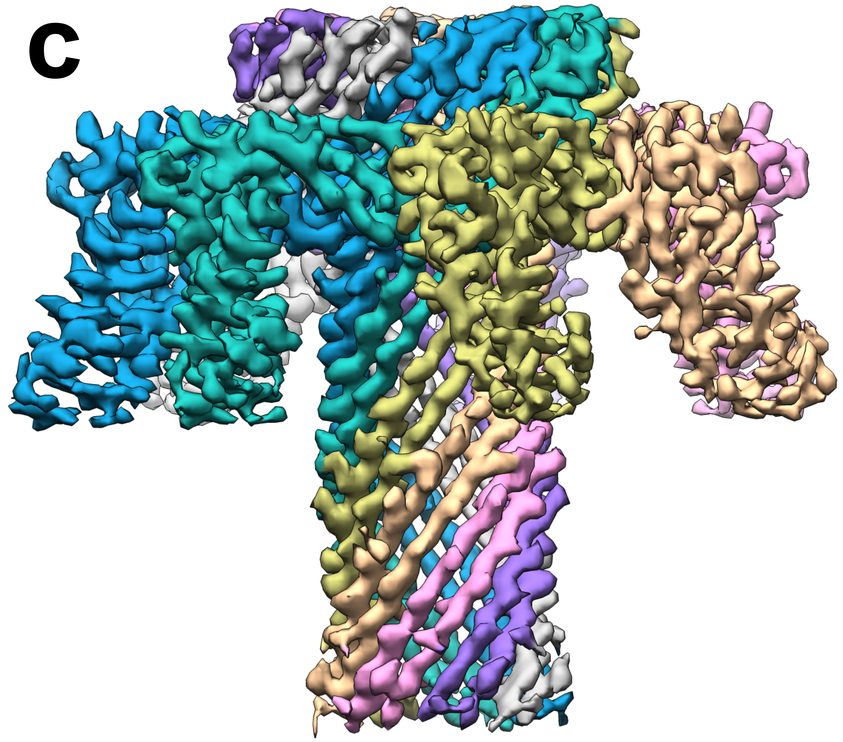
c

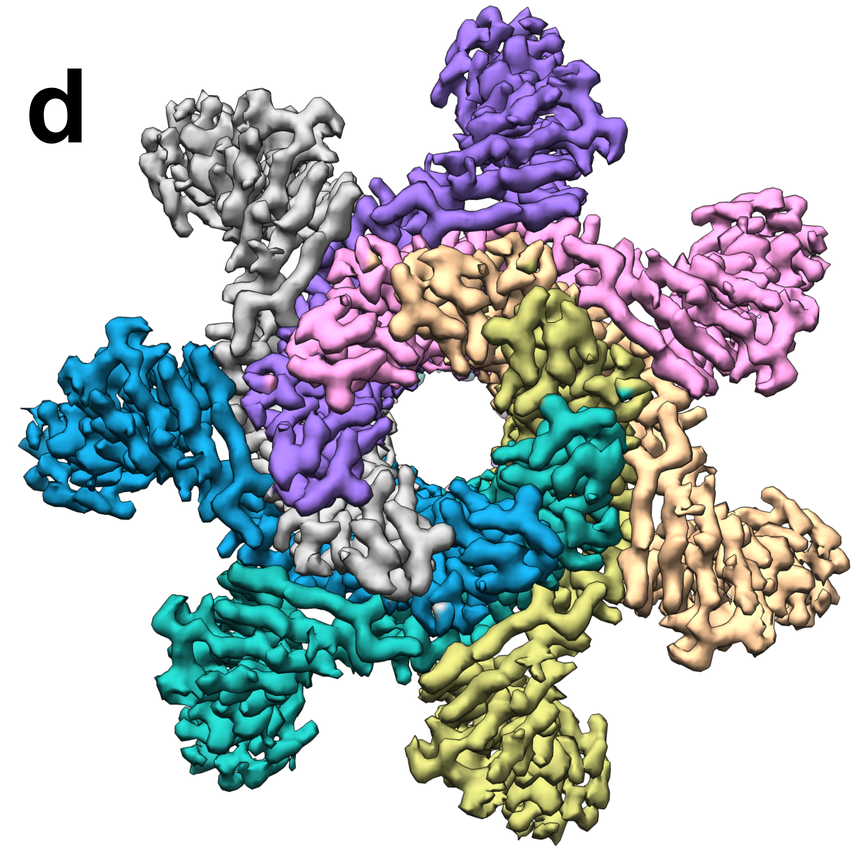
d

a

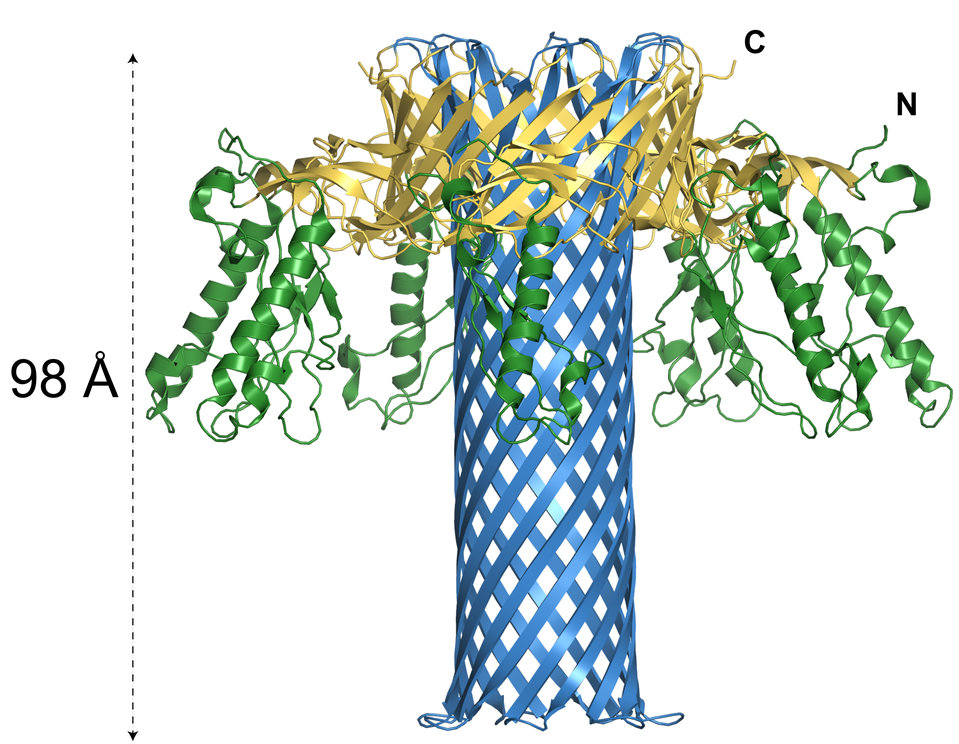
C
N
98 Å

b

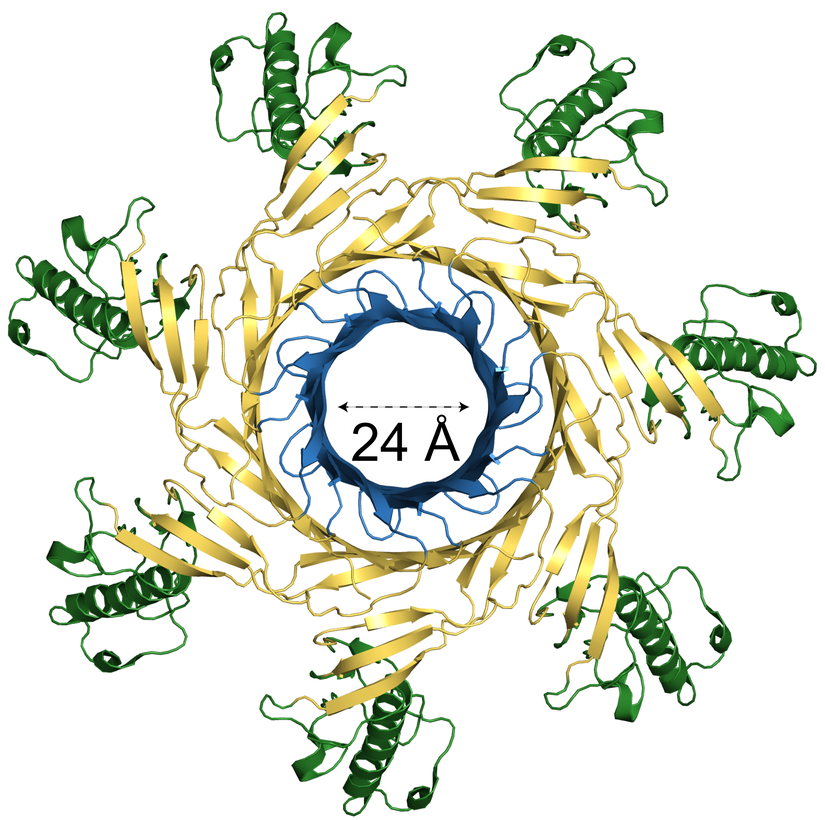
24 Å
120 Å

c

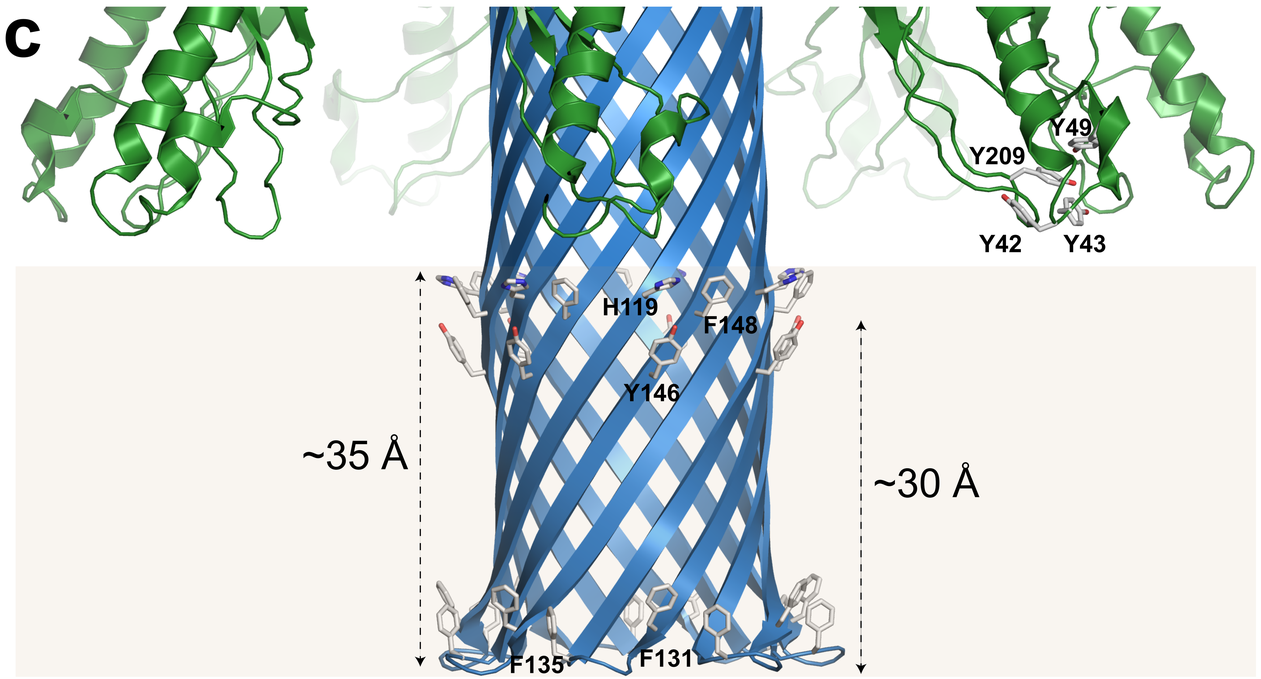
Y49
Y209
Y42
Y43
H119
F148
Y146
~35 Å
~30 Å
F135
F131

d

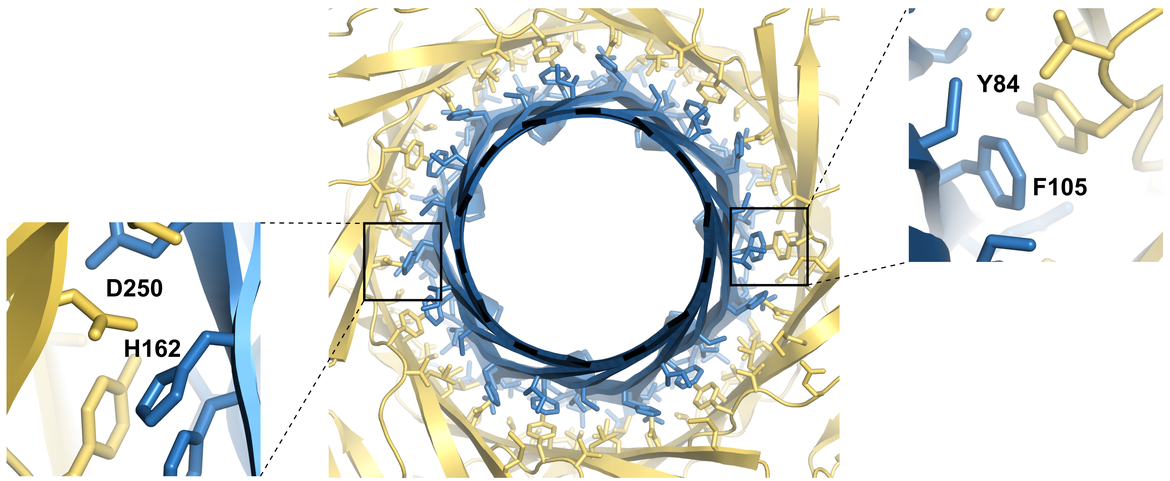
D250
H162
Y84
F105

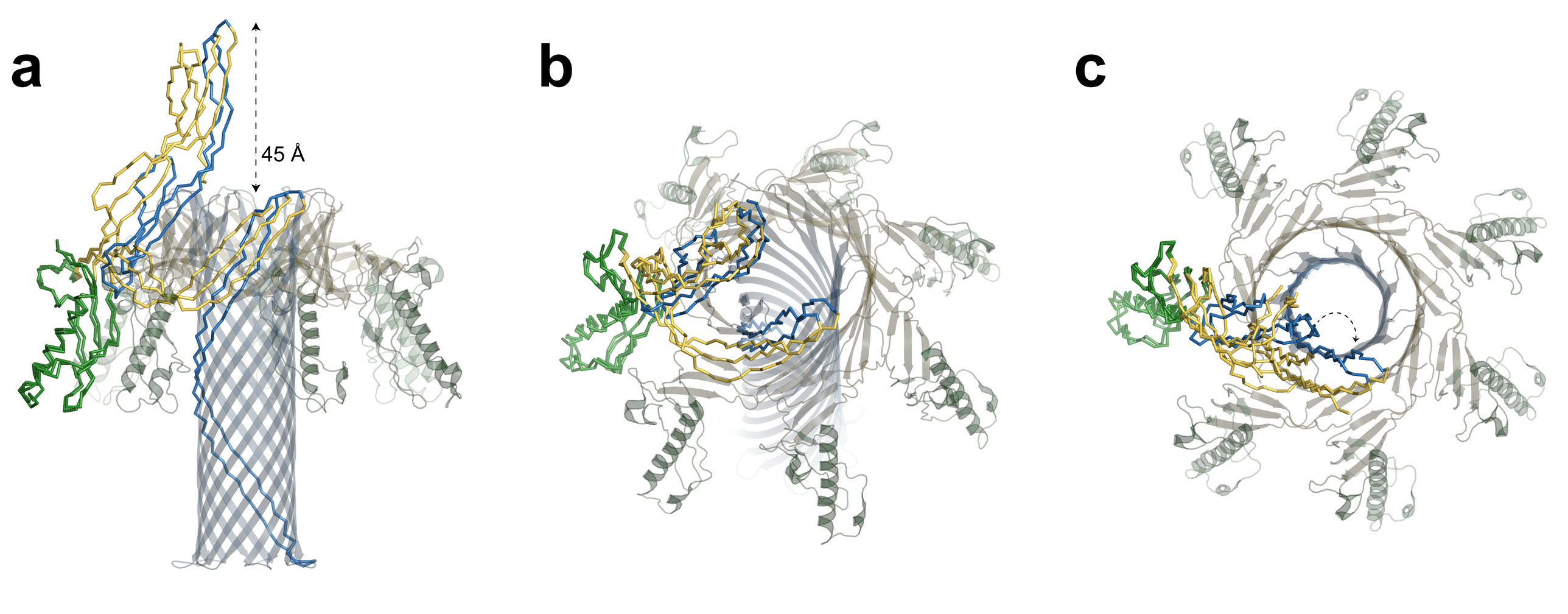
a
45 Å
b
c